



Cellular and Mitochondrial Toxicity of Raffinose Functionalized Graphene Oxide against Mouse Vital Organs

Parvaneh Naserzadeh^{1#}; Amir Jafari^{2,3#}; Atoosa Sharifi Shekarestalkhi^{2,3#}; Ali Maleki⁴; Rozhin Ahmadzadeh³; Faezeh Habibzadeh³; Masod Akhshik^{5,6}; Behnaz Ashtari^{2,3*}

¹Endocrine Research Center, Institute of Endocrinology and Metabolism, Iran University of Medical Sciences, Tehran, Iran.

²Cellular and Molecular Research Center, Iran University of Medical Sciences, Tehran, Iran.

³Department of Medical Nanotechnology, Faculty of Advanced technologies in Medicine, Iran University of Medical Sciences, Tehran, Iran.

⁴Catalysts and Organic Synthesis Research Laboratory, Department of Chemistry, Iran University of Science and technologies, Tehran, Iran.

⁵Centre for Biocomposites and Biomaterials Processing, University of Toronto, Canada.

⁶EPI Centre, University of Windsor, Canada.

*Corresponding Author(s): Behnaz Ashtari

Department of medical nanotechnology, Faculty of advanced technologies in medicine, Iran University of Medical Sciences, Tehran, Iran.

Email: ashtaribeh@gmail.com

#These authors have contributed equally to this paper.

Received: May 23, 2023

Accepted: June 09, 2023

Published Online: June 16, 2023

Journal: Journal of Nanomedicine

Publisher: MedDocs Publishers LLC

Online edition: <http://meddocsonline.org/>

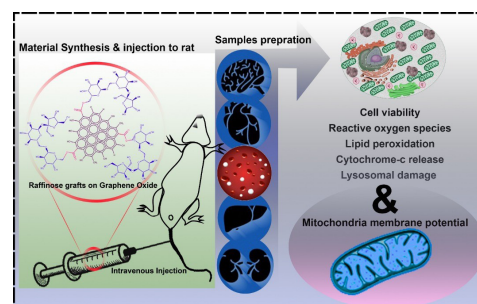
Copyright: © Ashtari B (2023). This Article is distributed under the terms of Creative Commons Attribution 4.0 International License

Keywords: Stress oxidative; Isolation mitochondria; Cell death signaling; Mitochondria pathway.

Abstract

Functionalized Nanoparticles (FNPs) using small or macromolecules have attracted research interest in targeted drug/gene delivery, tissue engineering, and imaging applications. The raffinose trisaccharide is the smallest raffinose oligosaccharides that has been used in fish's dietary supplements. Trisaccharides usually attached at the edge of Graphene Oxide (RafGO) nanosheets. In this study, cellular and mitochondrial toxicity of RafGO nanosheets was investigated in vital organs of the mouse. RafGO nanosheets induced stress oxidative in brain, liver, heart, kidney and B-lymphocytes cells and induce a dose dependent toxicity. We have detected Reactive Oxygen Species (ROS), glutathione content (GSH, GSSG), lysosome damage (redistribution of acridine orange), and mitochondrial membrane potential (MMP) and Cytochrome c. In this study we have also evaluate RafGO nanosheets induced cellular toxicity pathway and death signaling.

Graphical abstract



Cite this article: Naserzadeh P, Jafari A, Atoosa Sharifi S, Maleki A, Ahmadzadeh R, et al. Cellular and Mitochondrial Toxicity of Raffinose Functionalized Graphene Oxide against Mouse Vital Organs. J Nanomed. 2023; 6(1): 1062.

Introduction

Today nano-scale biomaterial has been studied for newly developed specific characteristics with the applications in biomedical devices. The variation in the characteristics have been related to size, charge, morphology, shape, doping agents and chemical moieties. Study of the nanosized materials, especially carbon-based one is thriving in the fields like: therapeutic carriers for targeted delivery, imaging features (e.g., quantum dots), biosensor, photothermal therapy and tissue engineering. Graphene is a single-atom-thick, two-dimensional sheet of hexagonally arranged carbon atoms [1,2]. The unique physicochemical properties of graphene-based material in conjugation with a broad range of its potential applications has been reviewed by Wang et al [3]. There are reports of graphene and its derivatives cytotoxic effects on both bacteria and mammalian cells [3]. In one of these reports, the intermediate-term effects of the nanosheets were studied on a mouse model and tracked for 21 days after the exposure. In this study it was concluded that nanosheets are associated with moderate lung injury and fibrosis, which can be mitigated by dispersing nanosheets in biocompatible molecules [4]. In another in-vivo research in *C. Elegans* model, the modified graphene oxide with PEGylated poly-L-lysine (electrostatic adsorption), (GO/PP) showed a relatively weak ROS formation. In this study it was concluded that the GO/PP induced decomposition of H_2O_2 and accelerated OH production and ROS formation under thermal stress condition rises and leads to the mitochondrial toxicity [5]. One of the interesting research projects studied the effect of Graphene Oxide (GO) in saline solution and its interactions with the membrane-bound cytochrome-c of *E.coli*. GO ability in transporting electrons from the respiratory chain and creating superoxide anions ($O_2^{\bullet-}$) lead to GO reductions; however, coating GO with bovine serum albumin (BSA) stopped GO's reduction. From all above it was concluded that by inhibiting direct assess of GO via macromolecules such as BSA they can increase stability and biocompatibility and reduce the toxicity [6]. In another interesting application, under the oxidizing environment, (GO)-Fe (III) complex was used as an artificial cytochrome-c that can have a selective photo-reduce toxic effects [7]. The collaboration of GO on the toxicity of other materials has been studied as well, for example, it has been illustrated that the developmental toxicity of TDCIPP on zebrafish in the presence of GO increases. Here the exposure of TDCIPP decreased activities of MRC enzymes and ATP while both engage in confronting GO. Overall GO nanosheets has a mitigating effect and reduces the adverse toxicity [8].

Raffinose is the smallest member of the raffinose family oligosaccharides which can be found in various plants and it was first extracted from Eucalyptus manna by Johnston in 1843 [9]. Raffinose is related to the regulations of the environmental stresses [10], it has applications in dietary supplements for fishes, OH scavenging activity [11-13], cryopreservation [14], aerosolization, hygroscopic effects that improves drugs characteristics [15] and as an excipient (protein stabilizer) [16-19].

There are two main methods to functionalize GO, on one hand is the non-covalent functionalization methods such as weak hydrophobic and π - π stacking interactions that are mainly being responsible for the attachment of the (bio) molecules or polymers. On the other hand, there are covalent bonding as well, which is the oxygen-based functional groups on the GO sheets are bonded to the organic matter. In term of interaction, the electrostatic interactions between biomolecules' functional

groups and the hydrogen bond, π - π -stacking and hydrophobic interactions are possible models of interactions that were recently reported for the GO [20]. Non-covalent interaction mostly meets the drug delivery needs but going through covalent reactions like etherification [21]. Beyond the probable reaction types, it is very important what kind of (bio) molecules is attached to the GO surfaces. For example, in 2018, Bidram and et al. conjugated GO with polyethylene glycol (PEG-FA) and (PEG-RGD) which led to internalization of both modified GO by the tumor cells and resulted in a less cytotoxicity for noncancerous cells [22]. If graphene oxide is toxic and able to induce dose dependent toxicity in cancer cells, how it is possible to work on graphene-based material in biomedical engineering? The simple answer is in the modifications, which might give them different properties and readers need to think of each modified GO as a different material with different properties.

On the mechanism of the toxicity beside from what has mentioned there is another aspect that has been mentioned elsewhere [23,24]. The DNA binding damages through complex forming mechanism, not only damages the animal and human cell lines; and also, sharp edge damages of nanosheets and nanopillars on bacterial membrane. In this mechanism the membrane mechanically ruptured or deformed upon the higher adhesion energy or energy balance respectively [25]. The accumulation of oxidative stress proteins, in bacteria, has near the GO sheets those bonds with neighboring lipid rafts, deactivates endocytosis, and causes metabolic deficiency. In silico studies concluded that sharpened edges of nanosheets could act like 'blades' that is extracting the phospholipid molecules from the lipid bilayers over its own surfaces. This blade exacerbates the loss of cell membrane integrity which followed by extraction-induced deformation [23]. This induced deformation has been explained with the membrane wrapping in endocytosis of various nanoparticles. Effective reduction of this toxicity in GO is also through functionalization with large or small molecules which can decrease the sharpness of the graphene oxide on the edges. In a study, researchers found that kaolin coagulations with graphene oxide in water, reduces the number of macronucleus deformities and adverse effects (low survival and growth rates), higher chemotaxis and lower galvanotaxis. In this study, we have demonstrated that the raffinose graphene oxide despite the advantageous properties of self-standing raffinose, still induce toxicity in brain, liver, heart, kidney and the B-lymphocytes cells. This has been demonstrated via several methods including the cell viability, mitochondrial ROS formation, mitochondrial membrane potential, lipid peroxidation level, glutathione content (GSH and GSSG), Cytochrome c expulsion assay, and damage lysosome.

Materials and Methods

Chemical and Materials

For this study we have used Silver Nitrate ($AgNO_3$), N, N'-Dicyclohexylcarbodiimide (DCC), 4,4-Dimethylaminopyridine (DMAP), Graphite fine powder extra pure (Merck, Germany), Sodium Nitrate ($NaNO_3$), Sulfuric Acid (98%), Potassium Permanganate merck, Hydrogen Peroxide. We also used MTT (3-[4,5-dimethylthiazol-2-yl]-2,5-diphenyltetrazolium bromide) to assay activity of mitochondrial complex II (succinate dehydrogenase). The formazan crystals were dissolved by Dimethyl Sulfide (DMSO). We evaluated ROS generation and MMP by 2',7'-Dichlorofluorescein Diacetate (DCFH-DA) and Rhodamine 123 (Rh 123) probes. For the evaluation of lipid peroxidation, Tetramethoxypropane (TEP) method was utilized. GSH and

GSSG were determined by OPA and NEM probes. Lysosomal membrane integrity was analyzed by acridine orange and Quantikine Rat/Mouse Cytochrome c Immunoassay kit (Minneapolis, MN). We used different buffers including Tris-HCl, sucrose, MgCl₂, KCl, MnCl₂, potassium phosphate 2-aminoethylether- N, N, N', N'-tetraacetic acid (EGTA), Ethylene ediamine tetra acetic acid (EDTA) and Na₂HPO₄ and Quantikine kit for released of cytochrome c. All chemicals were of analytical and/or HPLC grade.

Instrument

UV-Vis spectrums were obtained by Jenway 6705 UV-Visible Spectrophotometer. FTIR tests were done by Bomem MBB MB100 using KBr. DLS and Zeta Potential were measured by Malvern model MAL1041966. Fluorometry performed in Shimadzu RF-5000, Japan; and MTT assay was performed in finite 200 M ELISA reader (TECAN). Flow cytometry was performed using a BD Biosciences FACS Calibure TM flow cytometer.

Synthesis of the RafGO nanosheets

We have used the method explained (10.1021/acs.iecr.7b00182) to synthesize graphene oxide from graphite fine powder. Briefly, a beaker containing 20 mL H₂SO₄ and 0.5 g NaNO₃ is placed on a stirrer and heated to 66 °C. Then quickly 1 g of graphite fine powder was added to the solution and with gentle proportion solution was mixed for about 1 hour. The beaker containing the above solution was sonicated for 30 minutes in the bath provided with temperature of 0°C. Next, while stirring the solution with a spatula, 3 g of potassium permanganate (KMnO) was gradually added to the beaker. Then the beaker kept overnight at room temperature followed by adding 50 mL of a mixture of water/H₂O₂ (2/1 ratio) which induce a color change from black to brown. Finally, solution centrifuged at 4000 rpm for 3 min and washed till excessive KMnO₄ eliminated (checked with testing AgNO₃ precipitation using the supernatant. For grafting raffinose molecules on the GO, 10 mL GO (which contain 0.024g GO) added to a solution of 0.074g DCC and 0.005g DMAP dissolved in 50 mL 96% alcohol. Later, 0.025g of raffinose added to the solution while mixing gently on a magnetic stirrer for 48-hour at room temperature. The resulting powder was washed with distilled water and 96% EtOH (ethyl alcohol, also known as ethanol) three times and then dried in an oven at 60°C.

Fourier Transform Infrared Spectroscopy (FTIR)

Based on the presented FT-IR spectra, it was confirmed that the RafGO nanosheets were successfully synthesized. The prominent adsorption peaks of GO are at about 3434.5 cm⁻¹ which is attributed to the hydroxy group, 1625 cm⁻¹ which is attributed to carbonyl and 1700.5 cm⁻¹ which is attributed to C=O bonds of the carboxyl groups [26]. The FT-IR spectrum of RafGO represent the emerging new peak at 1725 cm⁻¹ that stands for ester bond formation. Moreover, the narrow sharp absorption peak at 3425 cm⁻¹ accounts for the presence of raffinose -OH groups indicating the reaction between COOH-edge groups and raffinose. In addition, the peaks of 996 cm⁻¹ confirms the COC link, asymmetric stretching of the furanose ring in raffinose molecules and also located small intensity at 895 cm⁻¹ is attributed to β-configuration of C-1-H(β) bending modes [9].

Scanning Electron Microscopy

Scanning Electron Microscopy (SEM AIS2 100, Seron Technology, South Korea) was used for morphological and topological investigations of the prepared nanosheets and scaffolds. In

this regard, the surface was coated with a thin layer of gold using a sputter coater (SC7620, Quorum Technologies, England) with accelerating voltage of 20kV. Then scaffolds were placed on the copper network of microscope and covered by carbon before imaging.

Animal model

Male mice (28±2 g) were fed with a normal standard chow diet and tap water ad libitum. All experiments were conducted according to the ethical standards and protocols approved by the Committee of Animal Experimentation of Shahid Beheshti University of Medical Sciences, Tehran, Iran. For tail vein injection (IV), 80 mice were randomly divided into eight groups (n = 10 for each group). The mice were injected via the tail vein with phosphate-buffered saline (PBS)-dispersed S-GO (dead/total) at dosages of 1(n=10:10), 5(n=10:10), 10(n=2:10), 15(5:10), 20(n=7:10), 25(n=9:10) and 30(n=10:10) mg/kg. We choose LD50 dosage (5mg/kg) for our project. After IV injection the animals were decapitated, brain, heart, liver and kidney were quickly excised, pooled, and rinsed using isotonic saline buffer. These samples were used for the isolation of cell and mitochondria as described below.

Experimental animal design

Samples were divided into 2 groups which: Group 1; control without RafGO nanosheets. Group 2; test with RafGO nanosheets.

Collection blood cells

Animals were euthanized with an intracardial injection of 1 mg/kg gallamine triethiodide (Specia, Paris, France) under general anesthesia. Before euthanasia, 1 mL of peripheral blood was collected from the tail vein. The peripheral blood samples were stained with Giemsa staining method for further evaluation.

Isolation of cells

Preparation of brain cells

Brain cells were prepared from the mice brain tissue. The mice were anesthetized with CO₂ and open skull mice picking up brain. 10% (w/v) Homogenate of brain tissue were centrifuged at 1000 g for 10 min. The supernatant centrifuged at 17000 g for 55 min. We showed different layer in supernatant; first layer between 0.32 and 0.8M sucrose centrifuged for 10000 g at 60 min. Second layer between 0.8 and 1.2M sucrose diluted with equal vol. of water centrifuged for 10000 g at 60 min [27].

Preparation of liver cells

The liver was carefully removed, transferred to a beaker containing 10-20 mL of enzyme medium at 4°C, and broken up with a blunt spatula. Additional enzyme medium was then added to bring the volume of the suspension to 50 mL. The suspension was divided into two equal portions and transferred to 250 mL conical flasks, which were shaken at 37°C for 15 min and in order to keep pH at 7.4 sodium bicarbonate solution was used. The incubation of the suspension served to break up cell clumps and, more important, to digest isolated nuclei and damaged cells. The suspension was filtered through two layers of nylon mesh and the cells were separated from debris by centrifuging at 50 g for 2 min. The supernatant was removed, and the cells were resuspended in fresh medium at 4°C. In some experiments, an additional step which appeared to bring about further improve-

ment in cell yield was included. After perfusion of the liver till it was of soft consistency, the enzyme medium was replaced with a medium containing calcium and magnesium-free Hanks' solution including 2 mM ethylenediaminetetraacetate (EDTA), pH 7.4. Perfusion was continued for 10 min and the remainder of the procedure was carried out as described previously [28].

Preparation of heart cells

The mice were killed by stunning and cervical dislocation, the heart removed quickly and placed in ice-cold bicarbonate buffer of the same composition as the perfusion fluid until beating ceased, followed by transferring to a tared container containing cold buffer and weighed. Perfusion was continued for a period of 5-16 min per grams of heart weight. Incubation of the tissue slices continued at 36°C until dispersion was achieved by gentle agitation in 10 mL vials. The resulting cell suspension was filtered and centrifuged at room temperature for 1 min at 22 g, then washed once by resuspension in 20 mL albumin-free buffer followed by centrifugation. The washed cell pellets were resuspended in a total of 20 mL. These suspensions were gassed at regular intervals with a 95% O₂, 5% CO₂ gas mixture [29].

Preparation of kidney cells

Mice renal proximal tubule segments were isolated and employs collagenase digestion of the renal cortex followed by percoll density gradient centrifugation. This procedure yielded a preparation primarily consisting of proximal tubule fragments. Culture medium was RPMI 1640 were added. Tubule fragments were suspended in culture medium and plated onto collagen gel-coated (Sigma, Type I) plastic 12-(4.5 cm²) multi well plates [30].

Preparation of B-lymphocytes

B-lymphocytes were positively selected from the whole blood of mice using Dynabeads M-450 coated with anti-CD19 mAb as described previously. Briefly, platelet-depleted buffy coats (50 ml) were mixed with 0.01 M EDTA in 25 ml RPMI 1640. Dynabeads M-450 Pan B were added to the cell suspension using a target-to-bead ratio of 1:10. The mixture was incubated for 30 min at 4°C, and rosette cells were captured using a samarium cobalt magnet. To obtain a pure B cell population the cell rosettes were washed seven times in 10 ml RPMI 1640 with 1% FCS. Detachment of B cells by overnight incubation Detachment of cells from Dynabeads M-450 Pan B by overnight culture was performed by incubating rosettes in RPMI 1640 with 1% FCS for 16-20 h in a CO₂ incubator. During this incubation the Dynabeads detached from the cells and the purified B lymphocytes were harvested after attracting the beads to the magnet. B lymphocytes were isolated from PB buffy coats by positive selection using anti-CD19 coated magnetic beads (Dynabeads M-450 Pan B; DYNAL, Oslo, Norway). Cells (1 X 10⁶ ml) were cultured in RPMI 1640 (GIBCO, Grand Island, NY) supplemented with penicillin, streptomycin, and 1% fetal bovine serum [31].

Cellular toxicity assay

Cell viability

The RafGO nanosheets were utilized to evaluate their reaction via measuring succinate dehydrogenase (complex II) activity [32].

Reactive oxygen species

In this experiment, isolated cells were placed in respiration

buffer. Afterwards, DCFH (Fluorescent probe used for ROS measurement) was added (final concentration, 10 μM) to cellular suspension and next incubated for 15min at 37°C. In the next step, the fluorescence was measured using Shimadzu RF-5000U fluorescence spectrophotometer at the excitation and emission wavelength of EXλ= 488 nm and EMλ=527 nm [32].

Glutathione redox state

The reduced glutathione (GSH) and oxidized glutathione (GSSG) is the most important scavengers of ROS that can be utilized as a biomarker of the redox balance in cellular oxidative stress. GSH and GSSG were measured at 540 nm at 10 min time intervals with an ELISA reader (Tecan, Rainbow Thermo, Austria) [33].

Lipid peroxidation

We employed Thiobarbituric Acid Reactive Substances (TBARS) assay for quantification of the products of the lipid peroxidation, which is Malondialdehyde (MDA). The results was recorded by ELISA reader (Tecan, Rainbow Thermo, Austria) at 540 nm [34].

Cytochrome-c release

Cytochrome c release was detected at 450 nm according to the instructions provided by the manufacturer of the Quantikines Rat/Mouse Cytochrome c Immunoassay Kit (Minneapolis, MN). All analysis stages were carried out using an ELISA reader (InfiniteM 200, TECAN) at desired concentrations in all groups.

Lysosomal damage

A lysosome is a membrane-bound organelle that comprises over 50 hydrolytic enzymes that are capable of breaking down various biomolecules. The lysosomes deal with garbage and recycling system of the cell by digesting unwanted materials in the cytoplasm both from outside of the cell (through endocytosis) and inside of the cell (through autophagy). Introduction of the damage or the permeabilization of the lysosome could activate cell death pathway. Lysosome malfunction may have different reasons such as reactive oxygen species. To determine the possible effects of the nanoparticles on mononuclear lysosomes, the cells were loaded with acridine orange [35].

Isolation of mitochondria and mitochondria membrane potential assay

Preparation of brain mitochondria

Brain mitochondria were isolated from the whole organs homogenized in 0.23 M mannitol, 0.07 M sucrose, 15 mM MOPS-KOH (pH 7.2) at a ratio of 9 ml of homogenization medium per 1 gram of tissue in a Potter homogenizer with a Teflon pestle. The homogenate was centrifuged at 700 g for 10 min and the supernatant at 8,000 g for 10 min to precipitate mitochondria that were washed in the same conditions [36].

Preparation of liver mitochondria

Liver mitochondria from all the groups were isolated using differential centrifugation. First, liver sections were excised from the euthanized rats, washed with 0.25 mol/L sucrose and homogenized and using MSHE at 4 °C for 5 min. The supernatant was then centrifuged at 10000 g for 10 min. Next, intact purified mitochondria were isolated using percoll to remove contaminating organelles and broken mitochondria. The pel-

let was then resuspended in 5 mL of MSHE supplemented with 20 mL of 30% percoll. This solution was spun at 95000 *g* in a centrifugation for 30 min. The fraction was then collected and washed twice with MSHE at 6300 *g* for 10 min. To remove the percoll, the purified mitochondria were washed twice using 150 mmol/L KCl and MSHE sequentially [37].

Preparation of heart mitochondria

Mice heart ventricles were frozen in liquid nitrogen, pulverized, and then homogenized in isolation buffer. Then the homogenate soup went through centrifuge step at 600 *g* for 10 min, yielding a pellet consisting of nuclei and myofibrils and a supernatant containing mitochondria, endoplasmic reticulum, and cytosol. The pellet was washed twice in isolation buffer, re-suspended in nuclear extraction buffer, and centrifuged at 600 *g* for 10 min. The supernatant was then centrifuged at 5,000 *g* for 15 min. The pellet here consisted of crude mitochondria [38].

Preparation of kidney mitochondria

Kidneys were homogenized in a buffer containing 20 mM/L Tris/MOPS, 400 mM/L sucrose, and 2 mM/L EGTA. After initial centrifugation at 750 *g*, supernatants were collected and centrifuged at 8,000 *g* for 10 min. Pellet was then resuspended and centrifuged again at 8,000 *g* for 10 min [39].

Preparation of B-lymphocytes mitochondria

B-lymphocytes were lysed and isolated mitochondria from B-lymphocytes. Mitochondria were isolated from the B-lymphocytes by mechanical lysis and differential centrifugation. Briefly, B-lymphocytes were washed with cold PBS at 4 °C and centrifuged at 450 *g*. The pellet was resuspended in cold isolation buffer, and the cells were disrupted by homogenization. Non lysed B-lymphocytes and nuclei were sedimented by centrifugation at 750 *g* for 20 min. The supernatant was further spun at 10,000 *g* for 10 min twice. The pellet, contains the mitochondrial fraction, was suspended in assay buffer [31, 40] prior to protein concentration measuring with Bradford method which adjusted to 5 mg/mL of protein.

Mitochondria membrane potential

The Rhodamine 123 (Rh 123) redistribution technique was used for mitochondria membrane potential (MMP) measurement. Isolated mitochondria (normalized to 100 mg of mitochondrial protein) for brain, heart, liver, kidney and B-lymphocytes mitochondria were suspended in 1 mL of analysis buffer, then Rh 123 (10 μ M) was added. Mitochondrial fluorescence was analyzed via fluorimetry (Ex: 490 nm and EM: 535 nm) [32].

Statistical Analysis

Results are presented as means \pm SD and all statistical analyses were conducted via GraphPad Prism software, version 5. Assays were performed in triplicate and the mean was used for the statistical analysis. Statistical significance was determined using the one-way ANOVA test, followed by the post-hoc Tukey and Bonferroni tests. Statistical significance was set at $P < 0.05$.

Results

The synthesis of the GO and RafGO is confirmed by using the simple FTIR technique. The omitted peaks from the spec-

trum imply that Raffinose attached to the GO and the existence of other characteristic peaks in both GO and RafGO conforms the grafting successfulness (**Figure 1**). In addition, further morphological study with the FE-SEM was also used for the direct confirmation (**Figure 2**). The morphology of freestanding GO nanosheets was more crumpled and rippled and tolerated a pre-shrunk condition and underlying causes which is related to the exfoliation and restacking processes (**Figure 2**). As it was expected for the RafGO, intercalate space of the nanosheets was enlarged. Because of the functionalization, RafGO nanosheets showed maximized shrunk morphology, which were more separated (exfoliated). GO nanosheets layers vary between 21 to 36 nm, whereas for RafGO nanosheets layers are about 24 to 35 nm. After the physiochemical characterization, fluorescence imaging of blood cells (1×10^4 cells/well) was performed and the results are shown in **Figure 3**. Here you can compare the before and after the exposure to RafGO nanosheets for 60 min. We observed that the blood cell did not have any changed in morphology in mouse blood cells. Through the study of all the participant group, we have observed that RafGO nanosheets induced a significant decrease in cell viability in isolated cells from brain, liver, heart, kidney; however, we did not record any significant decreased viability ($P < 0.05$) in B-lymphocytes compared with the control group (**Figure 4**). As shown in **Figure 5**, RafGO nanosheets induced a significant increase in ROS product in isolated cells from brain, liver ($P < 0.01$), heart, kidney and B-lymphocytes in comparison to control group. Moreover, substantial decrease in cell GSH in RafGO nanosheets affected isolated cells from brain, liver ($P < 0.01$), heart ($P < 0.001$) was observed; however, we did not see a significant decrease ($P < 0.05$) in GSH in the kidney and B-lymphocytes compared with the control group (**Figure 6**). **Figure 7** shows RafGO nanosheets induced a significant increase in GSSG isolated cells from brain, liver ($P < 0.01$), heart ($P < 0.05$), and B-lymphocytes ($P < 0.05$) but no significant decreases in kidney compared with control group ($P < 0.05$). Condition for lysosome damage was slightly better, likewise, in **Figure 8**, RafGO nanosheets induced a significant increase in lysosome damage for isolated cells originated from the brain and the liver ($P < 0.01$) but this was not the case for the heart, kidney and B-lymphocytes in comparison with the control group. Cellular energy metabolism of the kidney (**Figure 9**) didn't change in comparison with the control group, however, a significant increase of Rh123 in isolated cells from the liver ($P < 0.05$), heart ($P < 0.01$) B-lymphocytes ($P < 0.01$) was observed. **Figure 10** illustrated that all isolated cells treated by RafGO nanosheets have a significant release of cytochrome-c ($P < 0.01$) when compared with the control group.

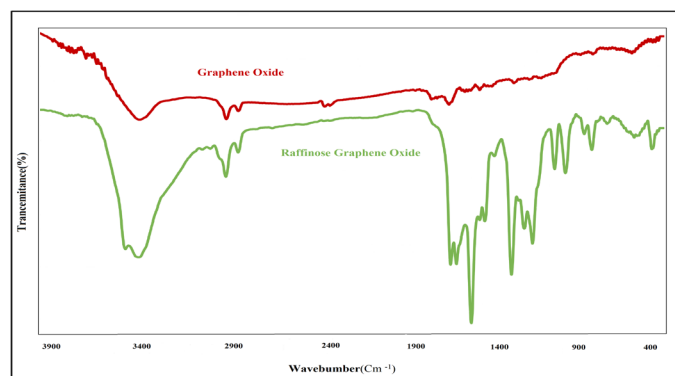


Figure 1: FT-IR spectra of graphene oxide (GO) and raffinose-GO powder.

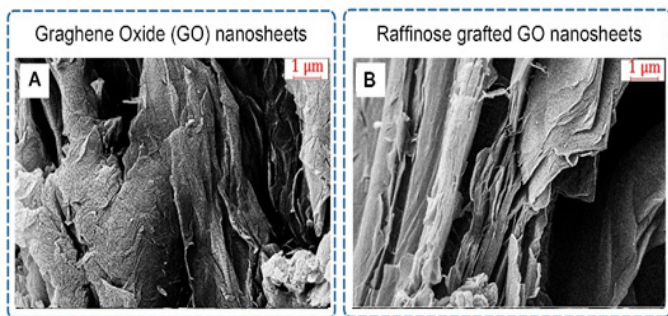


Figure 2: FE-SEM of the synthesized GO (A) and Raffinose nanosheets (B).

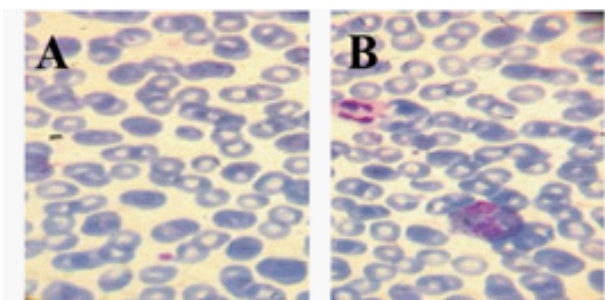


Figure 3: Imaging of blood cells before (A) and after (B) exposure of RafGO nanosheets. Pathology of blood cells.

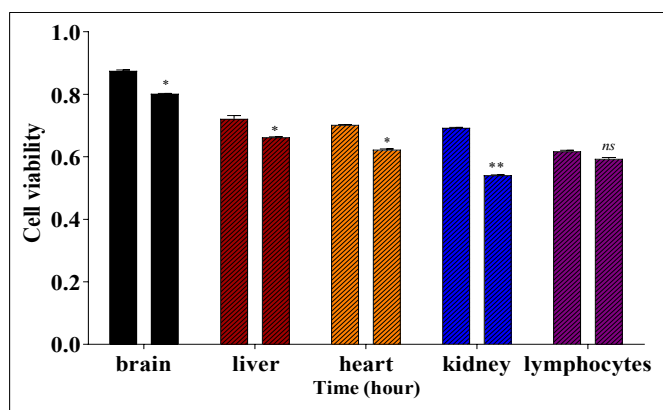


Figure 4: Cell viability assay of brain, liver, heart, kidney and B-lymphocytes before and after exposure RafGO nanosheets.

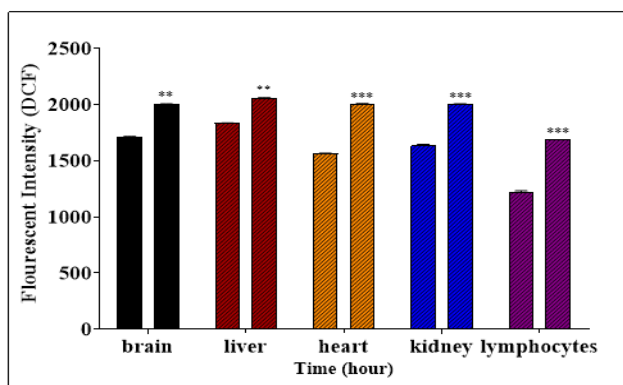


Figure 5: ROS assay on isolated cells from brain, liver, heart, kidney and B-lymphocytes before and after exposure RafGO nanosheets.

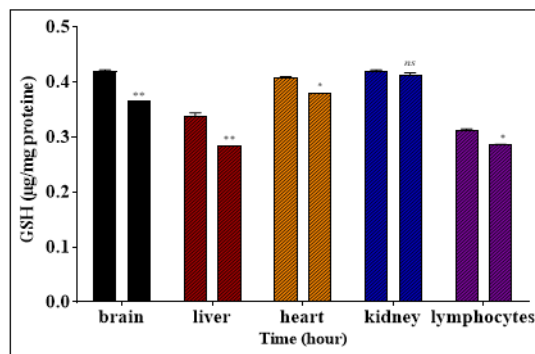


Figure 6: GSH assay on isolated cells from brain, liver, heart, kidney and B-lymphocytes before and after exposure RafGO nanosheets.

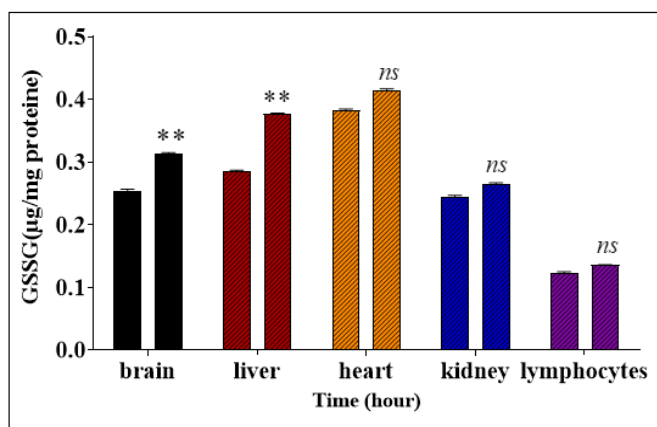


Figure 7: GSSG assay on isolated cells from brain, liver, heart, kidney and B-lymphocytes before and after exposure RafGO nanosheets.

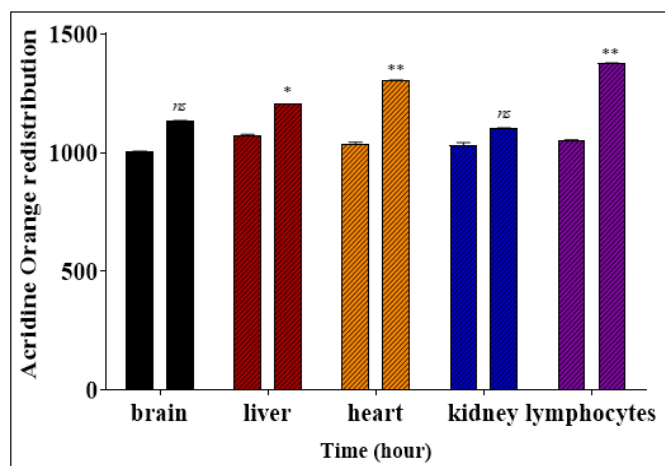


Figure 8: Lysosome damage assay on isolated cells from brain, liver, heart, kidney and B-lymphocytes before and after exposure RafGO nanosheets.

Discussion

The induction of the toxicity in the mitochondria of the different tissues through the manipulation of chemical moieties on nanoparticles' surfaces might shed light on chemically attachable candidate molecules which seem promising at first, in fact after testing in the simulated condition (e.g. in-vitro & in-vivo) probably target molecule successfully turn out to a good shelter against mitochondrial toxicity or otherwise, make it worse. In this research, we hypothesized that the probable

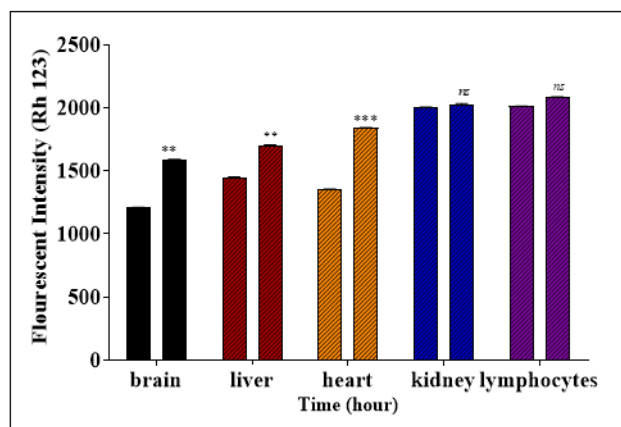


Figure 9: MMP assay on isolated cells from brain, liver, heart, kidney and B-lymphocytes before and after exposure RafGO nanosheets.

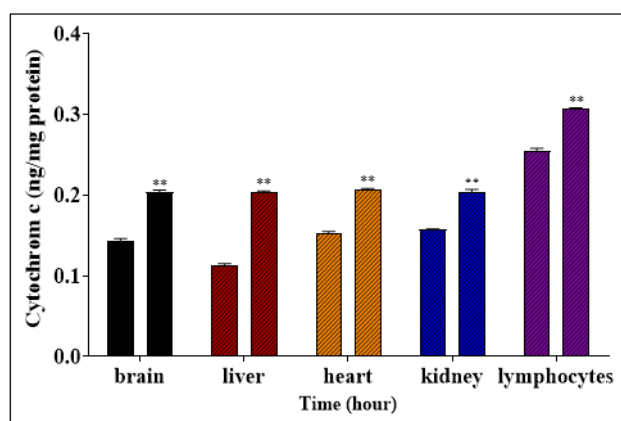


Figure 10: Cytochrome-c release assay on isolated cells from brain, liver, heart, kidney and B-lymphocytes before and after exposure RafGO nanosheets.

interactions between raffinose and graphene oxide especially in conjugated form, reduces the GO intrinsic toxicity especially at higher concentration. In other words, this experiment was designed to measure the effects of 60-minute exposure of RafGO on brain, heart, liver, kidney and B-lymphocytes, obtaining from the adult male mice. For this reason, the isolated blood cell and the suspension cells were washed. It's been shown that RafGO nanosheets in contact with blood cell, represents a low level of toxicity effect in cells (**figure 3**).

According to the literature, different mechanisms can cause nanoparticle or nanosheets toxicity in the animal body, several studies showed production of different level ROS via nanoparticles induced cytotoxicity [41]. Therefore, nanoparticles induced oxidative stress by producing ROS formation under biological conditions [42]

Interestingly, Moderate levels of ROS could induce different cellular events such as proliferative response, signal transduction, gene expression and protein redox regulation [43]. As we saw in **Figure 5**, RafGO nanosheets induced low-level toxicity in the brain, liver, heart and kidney cells and B-lymphocytes after exposure and the amount of ROS was revealed by fluorimetry. Despite the fact that MTT didn't provide any mechanistic information on mitochondrial malfunction and cell death signaling, this is one of the most used methods for determining cell viability [44]. Measuring succinate dehydrogenase (complex II) activity when exposed to the RafGO nanosheets showed a low level

of cytotoxicity in brain, liver, heart and kidney cells but not in B-lymphocytes. The results indicated that RafGO have a low level of toxicity in the mouse tissues. According to the literature, ROS formation induces oxidation of thiol groups in mitochondrial permeability transition (MPT) and make this pore to open [44].

Reduced glutathione (GSH) and oxidized glutathione (GSSG) are the most important scavengers of the ROS that can be utilized as the biomarkers of the redox balance in cells and cellular oxidative stresses. As shown in **Figure 6** and **Figure 7** the incubation of all the groups with RafGO nanosheets rapidly caused a slight decrease in GSH. Unlike GSH, the GSSG was significantly increased in the brain and liver cells. By putting our finding along with previous studies, it can be concluded that in terms of non-significant changes of ROS only mitochondria of the kidney cells remain safe and in terms of ROS and GSSG non-significant changes the heart, kidney and lymphocytes are safe.

The result of the lysosome experiment can be seen in **figure 8**. It was found that the lysosomes were moderately attenuated by the nanosheets for all groups except for the brain and kidney cells. The reason for this non-phagocytic by Non-phagocytic endocytosis like Caveolin-mediated endocytosis and this pathway does not merge with lysosomes. The other cells use other options for nanosheets uptake like phagocytic endocytosis (like endo-lysosomal pathways) which resulted in the material fuse with the lysosomes to form phagolysosomes, and by fusing nanosheets causes lysosomal dysfunction [45].

The ROS data (**Figure 5**) results in brain, heart, and liver show a convergence with MMP finding (**Figure 9**). Cells from the brain, heart, and liver, possibly most affected by the opening of MPT's pore because of lower tolerability or lower capacity of the GSH/GSSG system to resist against the ROS species. The most resistance cells against the ROS are kidney and to some extent B-lymphocytes and it can be concluded that the nanosheets were controlled by GSH/GSSG system and RafGO nanosheets remain inert in terms of the MMP. It had been illustrated that the cytochrome-c released happens to all treating groups in the cytosol fraction. The result of the released cytochrome-c is depicted in **figure 10**.

Despite the fact that GO edges had been grafted with raffinose almost reacted with all -COOH groups but in general it did not change the toxicological behavior in general. Therefore, it could be recommended the application of the larger molecules in this regard would be very beneficial and effective in inhibition of GO direct contact. Small molecules are not large enough to cover and stop the contact of the GO's direct contact with sub-cellular parts. It is also worth to mention that all of the participated groups-initiated ROS and cytochrome-c release eventually except for the brain and kidney that did not induce lysosome toxicity. In terms of decreasing GSH levels, heart, kidney, and lymphocyte cells weren't significant and the kidney cells GSSH level, confirmed the former results again. Kidney cells by using non-toxicities lysosomes even though induced ROS and cytochrome-have the lysosome intact and shows no toxicity levels at all. Moreover, the lymphocyte cells were similar in dead and live assay and also GSH level, also like kidney cells they did not show any MMP dysfunction. This means that the lymphocyte cells, like kidney cells were resistant against RafGO nanosheets. The liver cells showed more sensitivity and they were the only group that showed toxicity in any test and assay [46].

Conclusions

In our research, we studied the potential cellular and mitochondrial toxicity pathway of RafGO nanosheets on brain, heart, liver, kidney and B-lymphocytes cells *in vitro*. It was shown that the oxidative stress in brain, heart, liver, kidney and B-lymphocytes cells was directly involved. The reduced cell viability was associated with significant increases in the intracellular ROS level and toxic alterations in mitochondria and lysosomes. These effects depleted glutathione and the oxidative stress damaged mitochondrial membrane, causing cytochrome-c expulsion along with decreased ATP level, which ultimately led to cell death.

Reference

- Schweizer P, Dolle C, Dasler D, Abellan G, Hauke F, et al, Mechanical cleaning of graphene using in situ electron microscopy. *Nature Communications*. 2020. 11.
- Geim AK, AH. MacDonald, Graphene: Exploring carbon flatland. *Physics Today*, 2007; 60: 35-41.
- Wang W, Su H, Wu Y, Zhou T, Li T. Review-Biosensing and Biomedical Applications of Graphene: A Review of Current Progress and Future Prospect. *Journal of The Electrochemical Society*, 2019; 166: B505-B520.
- Budinger G, Duch MC, Urich D, Soberanes S, Chiarella S, et al., Graphene Oxide But Not Graphene Causes Severe Acute Lung Injury And Pulmonary Fibrosis In Mice. 2011. A2283-A2283.
- Zhang W, Wang C, Li Z, Lu Z, Li Y, et al., Unraveling Stress-Induced Toxicity Properties of Graphene Oxide and the Underlying Mechanism. *Advanced materials (Deerfield Beach, Fla.)*. 2012; 24: 5391-5397.
- Zhao H, Zhang C, Wang Y, Chen W, J J Alvarez P. Self-Damaging Aerobic Reduction of Graphene Oxide by *Escherichia coli*: Role of GO-Mediated Extracellular Superoxide Formation. *Environ Sci Technol*. 2018; 52: 12783-12791.
- Chen Z. Artificial Cytochrome c Mimics: Graphene Oxide-Fe(III) Complex Coated Molecularly Imprinted Colloidosomes for Selective Photoreduction of Highly Toxic Pollutants. *ACS Applied Materials & Interfaces*. 2020.
- Zou W, Zhang X, Ouyang S, Hu X, Zhou Q. Graphene oxide nanosheets mitigate the developmental toxicity of TDCIPP in zebrafish via activating the mitochondrial respiratory chain and energy metabolism. *Sci Total Environ*. 2020; 727: 138486.
- Wiercigroch E, Szafraniec E, Czamara K, Z Pacia M, Majzner K, et al., Raman and infrared spectroscopy of carbohydrates: A review. *Spectrochimica Acta Part A: Molecular and Biomolecular Spectroscopy*. 2017; 185: 317-335.
- Davidson P, WQ Sun, Effect of sucrose/raffinose mass ratios on the stability of co-lyophilized protein during storage above the Tg. *Pharmaceutical research*. 2001;18: 474-479.
- Li T, Dong M, Xie W, Zhang Y, Tao D, et al., Kinetic properties of raffinose synthase from rice (*Oryza sativa* L.). *Food Bioscience*. 2018; 25: 39-43.
- Van den Ende, W, Multifunctional fructans and raffinose family oligosaccharides. *Frontiers in plant science*. 2013; 4: 247.
- Warmund MR, P Guinan, G Fernandez. Temperatures and cold damage to small fruit crops across the eastern United States associated with the April 2007 freeze. *HortScience*. 2008; 43: 1643-1647.
- Elliot GD, Wang S, Fuller BJ. Cryoprotectants: A review of the actions and applications of cryoprotective solutes that modulate cell recovery from ultra-low temperatures. *Cryobiology*. 2017.
- Zhao Z, Huang Z, Zhang X, Huang Y, Cui Y, et al., Low density, good flowability cyclodextrin-raffinose binary carrier for dry powder inhaler: anti-hygroscopicity and aerosolization performance enhancement. *Expert opinion on drug delivery*, 2018; 15: 443-457.
- Lin S, Li L, Li M, Gu H, Chen X. Raffinose increases autophagy and reduces cell death in UVB-irradiated keratinocytes. *Journal of Photochemistry and Photobiology B: Biology*. 2019; 201: 111653.
- Thangavelu RM, Ganapathy R, Ramasamy P, Krishnan K. Fabrication of virus metal hybrid nanomaterials: An ideal reference for bio semiconductor. *Arabian Journal of Chemistry*. 2020; 13: 2750-2765.
- Van den Ende W, Multifunctional fructans and raffinose family oligosaccharides. *Frontiers in Plant Science*. 2013; 4.
- Nishizawa A, Yabuta Y, Shigeoka S. Galactinol and raffinose constitute a novel function to protect plants from oxidative damage. *Plant Physiol*, 2008; 147: 1251-1263.
- Liu J, Fu S, Yuan B, Li Y, Deng Z. Toward a universal "adhesive nanosheet" for the assembly of multiple nanoparticles based on a protein-induced reduction/decoration of graphene oxide. *Journal of the American Chemical Society*. 2010; 132: 7279-7281.
- Stergiou A, Canton-Vitoria R, N. Psarrou M, P. Economopoulos S, Tagmatarchis N, et al., Functionalized Graphene and Targeted Applications-Highlighting the Road from Chemistry to Applications. *Progress in Materials Science*. 2020: 100683.
- Bidram E, Sulistio A, Cho HJ, Amini A, Harris T, et al., Targeted Graphene Oxide Networks: Cytotoxicity and Synergy with Anticancer Agents. *ACS Appl Mater Interfaces*. 2018; 10: 43523-43532.
- Tu Y, Lv M, Xiu P, Huynh T, Zhang M, et al., Destructive extraction of phospholipids from *Escherichia coli* membranes by graphene nanosheets. *Nature nanotechnology*. 2013. 8.
- Kryuchkova M, Fakhrullin R. Kaolin Alleviates Graphene Oxide Toxicity. *Environmental Science & Technology Letters*. 2018; 5: 295-300.
- Jenkins J, Mantell J, Neal C, Gholinia A, Verkade P, et al., Antibacterial effects of nanopillar surfaces are mediated by cell impedance, penetration and induction of oxidative stress. *Nat Commun*. 2020; 11: 1626.
- Ghafuri H, Joorabchi N, Emami A, Reza Esmaili Zand H. Covalent Modification of Graphene Oxide with Vitamin B1: Preparation, Characterization, and Catalytic Reactivity for Synthesis of Benzimidazole Derivatives. *Industrial & Engineering Chemistry Research*. 2017; 56: 6462-6467.
- Gray EG, Whittaker VP. The isolation of nerve endings from brain: an electron-microscopic study of cell fragments derived by homogenization and centrifugation. *J Anat*. 1962. 96: 79-88.
- Berry MN, DS Friend. High-yield preparation of isolated rat liver parenchymal cells: a biochemical and fine structural study. *J Cell Biol*. 1969; 43: 506-520.
- Powell T, DA Terrar, VW Twist. Electrical properties of individual cells isolated from adult rat ventricular myocardium. *J Physiol*. 1980; 302: 131-153.
- Hafez AA, Naserzadeh P, Ashtari K, Amir MM, Salimi A. Protection of manganese oxide nanoparticles-induced liver and kidney damage by vitamin D. *Regulatory Toxicology and Pharmacology*. 2018; 98: 240-244.

31. Salimi A, Roudkenar MH, Sadeghi L, Mohseni A, Seydi E, et al., Ellagic acid, a polyphenolic compound, selectively induces ROS-mediated apoptosis in cancerous B-lymphocytes of CLL patients by directly targeting mitochondria. *Redox biology*. 2015; 6: 461-471.
32. Rezaei M, Salimi A, Taghidusta M, Naserzadehb P, Goudarzi G, et al., A comparison of toxicity mechanisms of dust storm particles collected in the southwest of Iran on lung and skin using isolated mitochondria. *Toxicological & Environmental Chemistry*. 2014. 96(5): p. 814-830.
33. Sadegh C, Schreck R. The Spectroscopic Determination of Aqueous Sulfite Using Ellman's Reagent. *MURJ*. 2002. 8.
34. Shaki F, Hosseini MJ, Ghazi-Khansari M, Pourahmad J, et al., Toxicity of depleted uranium on isolated rat kidney mitochondria. *Biochimica et Biophysica Acta (BBA) - General Subjects*. 2012; 1820: 1940-1950.
35. Seydi E, Rajabi M, Salimi A, Pourahmad J. Involvement of mitochondrial-mediated caspase-3 activation and lysosomal labilization in acrylamide-induced liver toxicity. *Toxicological & Environmental Chemistry*. 2015; 97: 563-575.
36. Wang WX, Visavadiya NP, Pandya JD, Nelson PT, Sullivan PG, et al., Mitochondria-associated microRNAs in rat hippocampus following traumatic brain injury. *Exp Neurol*. 2015. 265: p. 84-93.
37. Li L, Lu DZ, Li YM, Zhang XQ, Zhou XX, et al., Proteomic analysis of liver mitochondria from rats with nonalcoholic steatohepatitis. *World journal of gastroenterology*. 2014; 20: 4778-4786.
38. Santulli G, Xie W, Reiken SR, Marks AR. Mitochondrial calcium overload is a key determinant in heart failure. *Proc Natl Acad Sci U S A*. 2015; 112: 11389-11394.
39. Gamboa, JL, Bojanowski MT, Gilliam A, Yu C, Roshanravan B, et al., Mitochondrial dysfunction and oxidative stress in patients with chronic kidney disease. *Physiol Rep*. 2016; 4.
40. Rotem R, Heyfets A, Fingrut O, Blickstein D, Shaklai M, et al., Jasmonates: novel anticancer agents acting directly and selectively on human cancer cell mitochondria. *Cancer Res*. 2005; 65: 1984-93.
41. Nel, A, Xia T, Madler L, Li N. Toxic Potential of Materials at the Nanolevel. *Science*, 2006; 311: 622.
42. Xia T, Kovochich M, Brant J, Hotze M, Sempf J, et al., Comparison of the abilities of ambient and manufactured nanoparticles to induce cellular toxicity according to an oxidative stress paradigm. *Nano Lett*. 2006; 6: 1794-807.
43. Halliwell B, JMC Gutteridge, *Free Radicals in Biology and Medicine*. 2007, Oxford University Press: New York.
44. MS, *in vitro* toxicology of nanoparticles. *Proceedings of the Workshop*, 2005.
45. Stern ST, Adisheshaiah PP, RM Crist, Autophagy and lysosomal dysfunction as emerging mechanisms of nanomaterial toxicity. *Part Fibre Toxicol*. 2012; 9: 20.
46. Jafari AA, Emami, Ashtari B. PC12 cells proliferation and morphological aspects: Inquiry into raffinose-grafted graphene oxide in silk fibroin-based scaffold. *Materials Science and Engineering: C*, 2021; 121: 111810.